Moiré-Tile Manipulation Induced Friction Switch of Graphene on a Platinum Surface

Zhao Liu,[*,†,‡,#] J.G. Vilhena,[*,¶,†,#] Antoine Hinaut,[†] Sebastian Scherb,[†] Feng Luo,[§] Junyan Zhang,[‖] Thilo Glatzel,[†] Enrico Gnecco,[⊥] and Ernst Meyer[*,†]

†*Department of Physics, University of Basel, 4056 Basel, Switzerland*

‡*School of Materials Science and Engineering, Nankai University, 300350 Tianjin, China*

¶*Departamento de Física Teórica de la Materia Condensada, Universidad Autónoma de Madrid, 28049 Madrid, Spain*

§*Tianjin Key Lab for Rare Earth Materials and Applications, Center for Rare Earth and Inorganic Functional Materials, School of Materials Science and Engineering, Nankai University, 300350 Tianjin, China*

‖*State Key Laboratory of Solid Lubrication, Lanzhou Institute of Chemical Physics, Chinese Academy of Sciences, 730000 Lanzhou, China*

⊥*M. Smoluchowksi Institute of Physics, Jagiellonian University in Krakow, 30-348 Krakow, Poland*

#*These authors contributed equally to this work.*

E-mail: zhao.liu@unibas.ch; guilhermevilhena@gmail.com; ernst.meyer@unibas.ch

Abstract

Friction control and technological advancement are intimately intertwined. In this respect, two dimensional materials occupy a unique position as they enable the realization of quasi-frictionless contacts from nano up to micrometers. However, the question arises of how to tune superlubric sliding. Drawing inspiration from

twistronics, here we propose to control superlubricity via moiré patterning. Friction force microscopy and molecular dynamics simulations unequivocally demonstrate transition from superlubric to dissipative sliding regimes for different twist degrees of graphene moirés on a Pt(111) surface triggered by the normal force. This follows from a novel mechanism at superlattice level where beyond a critical load moiré tiles are manipulated in a highly dissipative shear process intimately connected to the twist angle. Such dissipation mechanism not only bridges disparate sliding regimes in a reversible manner, but also provides a subtly intrinsic control of superlubricity.

Introduction

Understanding and controlling friction is arguably one of the oldest quests of mankind.[1,2] From the great pyramids of Giza[3] to car engines[4] and all the way down to micro-electro-mechanical devices, a detailed control of this ubiquitous phenomena closely followed our technological advancement. In this regard, two dimensional (2D) materials are no exception as besides remarkable electronic and optical properties,[5] they possess extraordinary tribological properties.[6,7] Notably, 2D materials enable the realization of near frictionless sliding contacts, via a mechanism known as structural superlubricity.[8,9] Its practical interest spurred a vibrant research[10–13] in an attempt to tune/control structural superlubricity either extrinsically (*e.g.* by strain[14] and electric fields[15]) or intrinsically (*e.g.* by graphene fluorination[16]). The first approach, despite offering the advantage of controlling friction via an external knob, suffers from various practical issues. Particularly, it often requires complex device preparation thus hampering its technological interest. Alternatively, intrinsic methods enable to alter friction in a variety of 2D materials,[12,13] but once the sample is prepared, the tribo-properties cannot be changed. Drawing inspiration from the tuning of electronic properties achieved by rotating stacked 2D materials[17] (so-called twistronics), we propose a third route here to control superlubricity of 2D materials based on moiré superlattice engineering.

Results and discussion

Single graphene monolayers (Gr) were grown over Pt(111) in ultra-high-vacuum conditions, and investigated by the atomic force microscopy (AFM) as described in the Methods (see Fig. S1). The Gr/Pt lattice mismatch (0.246 nm *vs.* 0.278 nm) and the weak interaction between the two materials allows stabilizing a variety of moiré patterns on the same substrate, as already reported in the literature.[18–20] The atomically resolved topographies in Fig. 1a reveal both the graphene lattice and the moiré patterns. By measuring the periodicity of the moirés ($L_{R\theta}$), we identify four different superstructures, namely: $\sqrt{67} \times \sqrt{67}$ (L_{R2^o} = 2.2 nm), $\sqrt{37} \times \sqrt{37}$ (L_{R6^o} = 1.5 nm), 4×4 (L_{R14^o} = 1.0 nm), and 2×2 (L_{R30^o} = 0.5 nm). Henceforth, these moirés are respectively referred to as R2^o, R6^o, R14^o and R30^o (*i.e.* the corresponding twist angle between the Gr and Pt lattices).

At low values of the normal force, F_N, the average friction force, F_F, and the lateral force maps are fully consistent with previous findings:[19,21] see Fig. 1b and, respectively, Figs. 2a and c for both the largest (R2^o) and smallest (R30^o) moiré considered, and Fig. S2 for other moirés. When the tip is scanned over these superstructures, the lateral force evolves as a saw-tooth profile as a function of the scanned distance. The profile has the periodicity of the Gr lattice and is modulated by the moiré periodicity (Fig. 2a). The modulation perfectly matches the surface waviness of graphene. As a topographic effect, it does not result in lateral force hysteresis when the tip is scanned backward along the same line.[21] The order of magnitude of the friction coefficient μ, as defined by the slopes of the F_F *vs.* F_N curves, never overcomes 10^{-3}.

This scenario breaks down as the normal force increases above well-defined thresholds values F_N^c (Fig. 1b). Not only the thresholds are found to depend on the twist angle, but also the friction coefficients. The larger the moiré, the lower is F_N^c (from 50 nN to 20 nN), and the higher is μ in the high-load regime (from 0.03 up to 0.3, approximately). The rather regular saw-tooth profiles observed in Figs. 2b and d suggest that part of the friction increase is caused by the sudden slip of the tip from one graphene lattice site to a neighbor one. This

well-known behavior is explained by the occurrence of elastic instabilities, which, on standard crystal surfaces, is activated above a specific load threshold.[22] The background modulations also become very irregular above threshold (Fig. S2), with the noticeable exception of the bright high-friction spots observed on the large moiré pattern in Fig. 2b, which are perfectly arranged with the symmetry of its superstructure. Most important: The superlubric regime is fully recovered upon unloading (Fig. S3), meaning that the surfaces are not damaged in the dissipative regime. This behavior suggests the moiré, whilst playing only a *passive* geometric role at low loads, can be switched into an *active* tribo-element above a critical load.

To unveil atomic details occurring at the moiré-tip interface, we have performed all atom molecular dynamics (MD) simulations on graphene flakes of 10×10 nm^2 physisorbed over Pt(111) at the two limiting twist angles, *i.e.* R30^o and R2^o (see Fig. 3 and Methods). A rigid diamond tip is then driven elastically along the graphene armchair direction at different loads whilst recording the accompanying lateral force. The results summarized in Fig. 3a show comparable trends with the AFM measurements for what concerns the average friction values. Specifically, both simulations and experiment exhibit a twofold dependence of the lateral force on the normal load, *i.e.* a superlubric regime at low loads and a dissipative regime at high loads with threshold values of about 20 nN and 40 nN respectively. In the superlubric regime, both F_F ($\sim$100 pN) and μ ($\sim 10^{-4}$) are comparable on the two moirés. Similarly to the experiment, the dissipative sliding response is markedly distinct at high loads (Fig. 3a), and the friction coefficient μ decreases when the moiré size increases.

At low loads ($F_N < 20$ nN) the simulations also show that the moiré can modulate the lateral force (left panels of Figs. 3c and d) whilst its average value barely changes (Fig. 3a). An atomic detailed picture of this process is provided in Supplementary Movies S1 and S2. Briefly put, the lateral force modulation is associated to topography changes occurring in the transition between two Gr/Pt stacking domains (for each given Gr/Pt moiré): (i) an energetically favorable stacking region (EFSR), where Pt atoms occupy the graphene hollow sites (moiré valley, see Fig. 3d inset), and (ii) an energetically unfavorable stacking region

(EUSR), where graphene carbon atoms are directly above Pt atoms (moiré peak). On both regions, the lateral displacement of the Gr carbon atoms and the associated lateral force modulation are negligible. Conversely, the regions between peak and valley show the largest displacements corresponding to the largest lateral force modulation (left panel of Fig. 3d). The connection between topography and lateral force modulation also explains why different moirés have different lateral force modulation – *e.g.* in contrast with the largest moiré ($R2^o$), the 0.5 nm periodicity of the smallest moiré ($R30^o$) is barely apparent in the lateral force (Fig. 3c). This picture is consistent with previous work by Liu *et al.*[21]

At high loads ($F_N > F_N^c$), MD simulations unveil a novel dissipation mechanism, which may be called 'moiré tile manipulation' (Supplementary Movie S3). Provided that the load is sufficiently high, we have indeed observed that the tip pressure can force the underlying graphene to remain in-registry with Pt(111) at all times. An extreme example is shown in the red-shaded area in Fig. 3d. This forced registry is accompanied by a moiré-tile stretching (Fig. 3e). During this process, the base value of the lateral force gradually increases (Fig. 3d right panel) until the tip reaches the energetically unfavorable stacking region (inset of Fig. 3d right panel). At this point, the in-plane deformation of the moiré-tile (Fig. 3e) is released in a major slip event (from Fig. 3f to g) and the moiré recovers its initial conformation (accompanied with the retract of graphene network). The moiré tile manipulation mechanism consistently explains: (i) why larger moirés yield at lower normal loads (as stress is distributed over more atoms) and (ii) why dissipation is larger for larger moirés (as the dissipative slip event relates with the reorganization of a larger amount of atoms). The difference with the compliant 2D contact so obtained and the rigid one at low loads is sharp. It allows us to distinguish between two friction regimes, which can be interchanged depending on the normal load. In contrast with the load-induced transition reported by Socoliuc *et al.* on bulk material surfaces,[22] this mechanism is characterized by threshold values which are one order of magnitude higher and are tunable by the orientation of the moiré pattern. It is also interesting to compare our results with those on Gr/h-BN

recently reported by Zhang *et al.*[23] The periodicity of the moiré superstructure investigated in that work is much larger (about 15 nm), and the authors have distinguished two different load dependencies on friction, depending on whether the AFM tip crosses more than one tile or not. Stick-slip occurs with the periodicity of the moiré superstructure in the former case, and with the periodicity of the Gr lattice in the latter. Similarly to our conclusions, a combination of in-plane stretching and snap-back behavior is supposed to be the reason for the first phenomenon, although this hypothesis is not substantiated by MD simulations.

Conclusions

In summary, the two-fold frictional response on different Gr/Pt moirés has been related to the moiré-tile stretching beneath the probing tip. This mechanism allows switching between superlubric and dissipative sliding regimes in a reversible manner by simply changing the normal force. The moiré size or, equivalently, the twist angle between graphene/Pt(111), has a key role in the mechanism as they determine the friction coefficients, and the critical load thresholds. In spite of significant irregularities observed in the experimental friction maps, the MD simulations presented here unveil a novel dissipation channel potentially present in other 2D materials.[11,12] Therefore, beyond remarkable electronic properties,[17] moirés could open the path to tribomechanical elements with tunable friction properties on the nanoscale.

Experimental Methods

Sample preparation.

Clean and flat Pt(111) single crystal (MaTeck GmbH, Germany) was in-situ prepared by alternated cycles of Ar^+ sputtering and annealing in ultra-high vacuum (UHV). Graphene was synthesized by dosing 4.5 L ethylene onto the hot Pt(111) substrate at 1200 K,[24,25] with a nearly full coverage of monolayer graphene.[26]

Atomic/Friction Force Microscopy experiments.

All the experiments were carried out by a custom-built UHV AFM at room temperature. The non-contact and the contact cantilevers (Nanosensor) were used for the topography and the friction force measurement, respectively. Bimodal nc-AFM with PPP-NCL cantilevers (the nominal spring constant $k_0 = 48$ N/m) was applied to combine the first flexural resonance ($f_1 = 170$ kHz with a quality factor $Q_1 = 3 \times 10^4$) and the torsional resonance ($f_t = 1.5$ MHz with a quality factor $Q_t = 1.2 \times 10^5$) detection to obtain the high-quality atomic resolution. For FFM measurement with PPP-CONT cantilevers (the nominal spring constant $k_0 = 0.2$ N/m and the resonance frequency $f = 12$ kHz), the normal forces and the lateral forces were calibrated with the sensitivity of the photodetector (obtained from the force-distance curve).[1] Then, the averaged friction force could be calculated from the area of hysteresis loops enclosed by the forward and backward lateral scanning curves divided by the total distance scanned. The cantilever dimensions used for force calibration above are measured by the scanning electron microscopy (Nova NanoSEM 230, Switzerland), especially with the tip radius of $10 \sim 15$ nm. The applied load was increased from 2 nN until the suddenly jumping friction forces (*i.e.* $F_N^{max} = F_N^c + 10$ nN), with the scanning speed of 10 nm/s for the whole experiments.

Molecular dynamics (MD) simulation details.

MD simulations were carried out using GROMACS-2019.4[27] simulation package in a hybrid GPU–CPU computing architecture.[28] All simulations were performed in the Canonical (NVT) ensemble where the number of atoms (N), volume (V) and temperature ($T = 300$ K) were held constant. The simulation parameters and algorithms used are: periodic boundary conditions, smooth particle mesh Ewald summation[29] with cubic spline interpolation of the electrostatic energy contribution and a real-space Coulombic cutoff of 1 nm. Interatomic Van der Waals interactions were also truncated at 1 nm. Previously, these parameters allowed obtaining a quantitative agreement with experiments to describe sliding

friction of a diamond tip over a graphene surface.[30] The dimension of the simulation box ($48.63574 \times 48.46434 \times 30.00000$ nm^3) largely surpassed the system size in all directions so spurious contributions from periodic images are avoided. A Langevin thermostat[31] was employed to keep the mean temperature at 300 K after rapid slip events. A damping rate of 1 ps^{-1} ensured that any excess heat was soon dissipated between such events. Equations of motion were integrated with an accurate and efficient leap-frog stochastic dynamics integrator[31] with a time step of 0.1 fs. Coordinates, forces and velocities of atoms were written every 100 ps, whilst the force was written every 0.02 ps.

Atomic level models and force-fields.

We considered a 25×25 nm^2 Pt(111) slab parallel to the XY plane, *i.e.* perpendicular to the Z axis. The slab is three layers thick and the bottom layer is kept fixed to mimic the effect of the rigid supports used in our experiments. As graphene (Gr), we consider a 20×20 nm^2 square flake. After equilibrating the coordinates of both Pt(111) and Gr in a preliminary 1 ns MD run, we placed the Gr on top of Pt(111) such that the angle between lattices is: R2^o so to reproduce largest moiré in agreement with prior works,[20] and R30^o so to reproduce smallest moiré. Additionally, in order to mimic the graphene pinning to the Pt(111) observed in experiments,[32] the four Gr edges are fixed (by freezing the coordinates of 6 atoms composing each edge) when sliding the tip over the Gr – note that different pinning conformations tested (*e.g.* line/point pinning) yielded similar results. For the tip, we used the same hard diamond tip which previously allowed us to unveil the role of water in graphene friction.[30] Namely, we considered a conically shaped diamond tip with a radius of 1.1 nm and a contact radius of 0.45 nm (the diamond is cleaved such that the (111) plane is parallel to the surface). The atomic interactions are described by classical force fields (GAFF[33] for diamond and graphene and INTERFACE-FF[34,35] platinum) that are known to accurately describe the mechanical,[30,36] and interaction energies, forces and diffusion energy barriers for the considered atom-types.[34,37,38]

MD simulation protocol.

Initially, each of the system components (Pt slab, graphene and tip) was equilibrated in 1 ns long gas-phase MD runs performed at 300 K, thus assuring that the starting configuration was a relaxed one. Subsequently, the graphene is placed on top of the Pt(111) in two different lattice angles (described in the former section) so to reproduce the smallest and largest moiré. Then the moiré is equilibrated in a subsequent 10 ns long MD run at 300 K. Afterwards, the diamond tip is positioned at a distance of 1.4 nm away from the surface. Then, the surface is indented at a velocity of 1 m/s whilst recording the indentation force. Subsequently, from the frames extracted at different normal loads, we slide the diamond tip over the graphene at a constant velocity of 1 m/s whilst recording the lateral force required to slide the tip using the pull algorithm available in GROMACS-2019.4.[27] The tip is driven along the slide direction with a spring of stiffness of 20 N/m, whilst motion along the other directions is restrained. Different sliding speeds and pulling stiffnesses did not change the overall conclusions.

Supporting Information

Figs. S1 to S5

Movies S1 to S4

Acknowledgement

Funding: We gratefully acknowledge the financial support by the Projects of International Cooperation and Exchanges from National Key Research and Development Program of China (No. 2021YFA1601004), National Natural Science Foundation of China (No. 51661135022), the FET-Open Program "Quantum-Limited Atomic Force Microscopy" (No.

828966), the European Research Council (ERC) under the European Union's Horizon 2020 Research and Innovation Program (No. 834402) as well as the Swiss National Science Foundation (SNSF), the Swiss Nanoscience Institute (SNI) and the University of Basel. The COST Action MP1303 is gratefully acknowledged. J.G.V. acknowledges the assistance and computing resources from Red Española de Supercomputación (RES-BSC) HPC computational facilities, funding from a Marie Sklodowska-Curie Fellowship within the Horizons 2020 framework (DLV-795286), the Swiss National Science Foundation (grant number CRSK-2 190731/1), Spanish CM Talento Program Project No. 2020-T1/ND-20306 and the Spanish Ministerio de Ciencia e Innovación Grant No. PID2020-113722RJ-I00.

Author contributions: Z.L. F.L. T.G. and E.M. conceived the original idea and the experiments. Z.L. A.H. and S.S. performed the AFM measurements and FFM experiments. J.G.V. conducted the numerical simulations. J.G.V., Z.L. and E.G. wrote the manuscript; E.M., J.Y.Z. and J.G.V. acquired the research funding. All authors discussed the results and revised the manuscript.

Competing interests: The authors declare no competing interests.

Data and materials availability: Data required to evaluate the conclusions here presented is fully provided both in the main manuscript and the supporting information.

References

(1) Bhushan, B. Nanotribology and nanomechanics. *Wear* **2005**, *259*, 1507–1531.

(2) Krylov, S. Y.; Frenken, J. W. M. The physics of atomic-scale friction: Basic considerations and open questions. *Phys. Status Solidi B* **2014**, *251*, 711–736.

(3) Fall, A.; Weber, B.; Pakpour, M.; Lenoir, N.; Shahidzadeh, N.; Fiscina, J.; Wagner, C.; Bonn, D. Sliding Friction on Wet and Dry Sand. *Phys. Rev. Lett.* **2014**, *112*, 175502.

(4) Erdemir, A.; Martin, J. M. *Superlubricity*; Elsevier, 2020.

(5) Liu, Y.; Weiss, N. O.; Duan, X.; Cheng, H.-C.; Huang, Y.; Duan, X. Van der Waals heterostructures and devices. *Nat. Rev. Mater.* **2016**, *1*, 16042.

(6) Vazirisereshk, M. R.; Ye, H.; Ye, Z.; Otero-de-la Roza, A.; Zhao, M.-Q.; Gao, Z.; Johnson, A. C.; Johnson, E. R.; Carpick, R. W.; Martini, A. Origin of nanoscale friction contrast between supported graphene, MoS2, and a graphene/MoS2 heterostructure. *Nano Lett.* **2019**, *19*, 5496–5505.

(7) Serles, P.; Arif, T.; Puthirath, A. B.; Yadav, S.; Wang, G.; Cui, T.; Balan, A. P.; Yadav, T. P.; Thibeorchews, P.; Chakingal, N., et al. Friction of magnetene, a non–van der Waals 2D material. *Sci. Adv.* **2021**, *7*, eabk2041.

(8) Dienwiebel, M.; Verhoeven, G. S.; Pradeep, N.; Frenken, J. W.; Heimberg, J. A.; Zandbergen, H. W. Superlubricity of graphite. *Phys. Rev. Lett.* **2004**, *92*, 126101.

(9) Berman, D.; Erdemir, A.; Sumant, A. V. Approaches for achieving superlubricity in two-dimensional materials. *ACS Nano* **2018**, *12*, 2122–2137.

(10) Kawai, S.; Benassi, A.; Gnecco, E.; Söde, H.; Pawlak, R.; Feng, X.; Müllen, K.; Passerone, D.; Pignedoli, C. A.; Ruffieux, P., et al. Superlubricity of graphene nanoribbons on gold surfaces. *Science* **2016**, *351*, 957–961.

(11) Song, Y.; Mandelli, D.; Hod, O.; Urbakh, M.; Ma, M.; Zheng, Q. Robust microscale superlubricity in graphite/hexagonal boron nitride layered heterojunctions. *Nat. Mater.* **2018**, *17*, 894–899.

(12) Li, S.; Li, Q.; Carpick, R. W.; Gumbsch, P.; Liu, X. Z.; Ding, X.; Sun, J.; Li, J. The evolving quality of frictional contact with graphene. *Nature* **2016**, *539*, 541–545.

(13) Lee, C.; Li, Q.; Kalb, W.; Liu, X.-Z.; Berger, H.; Carpick, R. W.; Hone, J. Frictional characteristics of atomically thin sheets. *Science* **2010**, *328*, 76–80.

(14) Zhang, S.; Hou, Y.; Li, S.; Liu, L.; Zhang, Z.; Feng, X.-Q.; Li, Q. Tuning friction to a superlubric state via in-plane straining. *Proc. Natl. Acad. Sci.* **2019**, *116*, 24452–24456.

(15) Yu, K.; Zou, K.; Lang, H.; Peng, Y. Nanofriction characteristics of h-BN with electric field induced electrostatic interaction. *Friction* **2020**, *9*, 1492–1503.

(16) Zheng, X.; Gao, L.; Yao, Q.; Li, Q.; Zhang, M.; Xie, X.; Qiao, S.; Wang, G.; Ma, T.; Di, Z., et al. Robust ultra-low-friction state of graphene via moiré superlattice confinement. *Nat. Commun.* **2016**, *7*, 1–7.

(17) Cao, Y.; Fatemi, V.; Fang, S.; Watanabe, K.; Taniguchi, T.; Kaxiras, E.; Jarillo-Herrero, P. Unconventional superconductivity in magic-angle graphene superlattices. *Nature* **2018**, *556*, 43–50.

(18) Enachescu, M.; Schleef, D.; Ogletree, D.; Salmeron, M. Integration of point-contact microscopy and atomic-force microscopy: Application to characterization of graphite/Pt (111). *Phys. Rev. B* **1999**, *60*, 16913.

(19) Chan, N.; Balakrishna, S.; Klemenz, A.; Moseler, M.; Egberts, P.; Bennewitz, R. Contrast in nanoscale friction between rotational domains of graphene on Pt(111). *Carbon* **2017**, *113*, 132–138.

(20) Gao, M.; Pan, Y.; Huang, L.; Hu, H.; Zhang, L.; Guo, H.; Du, S.; Gao, H.-J. Epitaxial growth and structural property of graphene on Pt(111). *Appl. Phys. Lett.* **2011**, *98*, 033101.

(21) Liu, J.; Zhang, S.; Li, Q.; Feng, X.-Q.; Di, Z.; Ye, C.; Dong, Y. Lateral force modulation by moiré superlattice structure: Surfing on periodically undulated graphene sheets. *Carbon* **2017**, *125*, 76–83.

(22) Socoliuc, A.; Bennewitz, R.; Gnecco, E.; Meyer, E. Transition from stick-slip to

continuous sliding in atomic friction: entering a new regime of ultralow friction. *Phys. Rev. Lett.* **2004**, *92*, 134301.

(23) Zhang, S.; Yao, Q.; Chen, L.; Jiang, C.; Ma, T.; Wang, H.; Feng, X.-Q.; Li, Q. Dual-Scale Stick-Slip Friction on Graphene/h- BN Moiré Superlattice Structure. *Phys. Rev. Lett.* **2022**, *128*, 226101.

(24) Sutter, P.; Sadowski, J. T.; Sutter, E. Graphene on Pt(111): Growth and substrate interaction. *Phys. Rev. B* **2009**, *80*, 245411.

(25) Johánek, V.; De la Ree, A. B.; Hemminger, J. C. Scanning tunneling microscopy investigation of the conversion of ethylene to carbon clusters and graphite on Pt(111). *J. Phys. Chem. C* **2009**, *113*, 4441–4444.

(26) Coraux, J.; Plasa, T. N.; Busse, C.; Michely, T., et al. Structure of epitaxial graphene on Ir(111). *New J. Phys.* **2008**, *10*, 043033.

(27) Abraham, M. J.; Murtola, T.; Schulz, R.; Páll, S.; Smith, J. C.; Hess, B.; Lindahl, E. GROMACS: High performance molecular simulations through multi-level parallelism from laptops to supercomputers. *SoftwareX* **2015**, *1-2*, 19–25.

(28) Páll, S.; Abraham, M. J.; Kutzner, C.; Hess, B.; Lindahl, E. Tackling Exascale Software Challenges in Molecular Dynamics Simulations with GROMACS. Solving Software Challenges for Exascale. Cham, 2015; pp 3–27.

(29) Darden, T.; York, D.; Pedersen, L. Particle mesh Ewald: An N·log(N) method for Ewald sums in large systems. *J. Chem. Phys.* **1993**, *98*, 10089–10092.

(30) Vilhena, J. G.; Pimentel, C.; Pedraz, P.; Luo, F.; Serena, P. A.; Pina, C. M.; Gnecco, E.; Pérez, R. Atomic-Scale Sliding Friction on Graphene in Water. *ACS Nano* **2016**, *10*, 4288–4293.

(31) Goga, N.; Rzepiela, A. J.; de Vries, A. H.; Marrink, S. J.; Berendsen, H. J. C. Efficient Algorithms for Langevin and DPD Dynamics. *J. Chem. Theory Comput.* **2012**, *8*, 3637–3649.

(32) Martínez, J. I.; Merino, P.; Pinardi, A. L.; Gonzalo, O.-I.; López, M. F.; Méndez, J.; Martín-Gago, J. A. Role of the pinning points in epitaxial graphene moiré superstructures on the Pt(111) Surface. *Sci. Rep.* **2016**, *6*, 20354.

(33) Wang, J.; Wolf, R. M.; Caldwell, J. W.; Kollman, P. A.; Case, D. A. Development and testing of a general amber force field. *J. Comput. Chem.* **2004**, *25*, 1157–1174.

(34) Heinz, H.; Ramezani-Dakhel, H. Simulations of inorganicbioorganic interfaces to discover new materials: insights, comparisons to experiment, challenges, and opportunities. *Chem. Soc. Rev.* **2016**, *45*, 412–448.

(35) Heinz, H.; Lin, T.-J.; Kishore Mishra, R.; Emami, F. S. Thermodynamically Consistent Force Fields for the Assembly of Inorganic, Organic, and Biological Nanostructures: The INTERFACE Force Field. *Langmuir* **2013**, *29*, 1754–1765.

(36) Tsai, J.-L.; Tu, J.-F. Characterizing mechanical properties of graphite using molecular dynamics simulation. *Mater. Design* **2010**, *31*, 194–199.

(37) Pawlak, R.; Vilhena, J. G.; Hinaut, A.; Meier, T.; Glatzel, T.; Baratoff, A.; Gnecco, E.; Pérez, R.; Meyer, E. Conformations and cryo-force spectroscopy of spray-deposited single-strand DNA on gold. *Nat. Comm.* **2019**, *10*, 685.

(38) Scherb, S.; Hinaut, A.; Pawlak, R.; Vilhena, J. G.; Liu, Y.; Freund, S.; Liu, Z.; Feng, X.; Mullen, K.; Glatzel, T.; Narita, A.; Meyer, E. Giant thermal expansion of a two-dimensional supramolecular network triggered by alkyl chain motion. *Commun. Mater.* **2020**, *1*, 8.

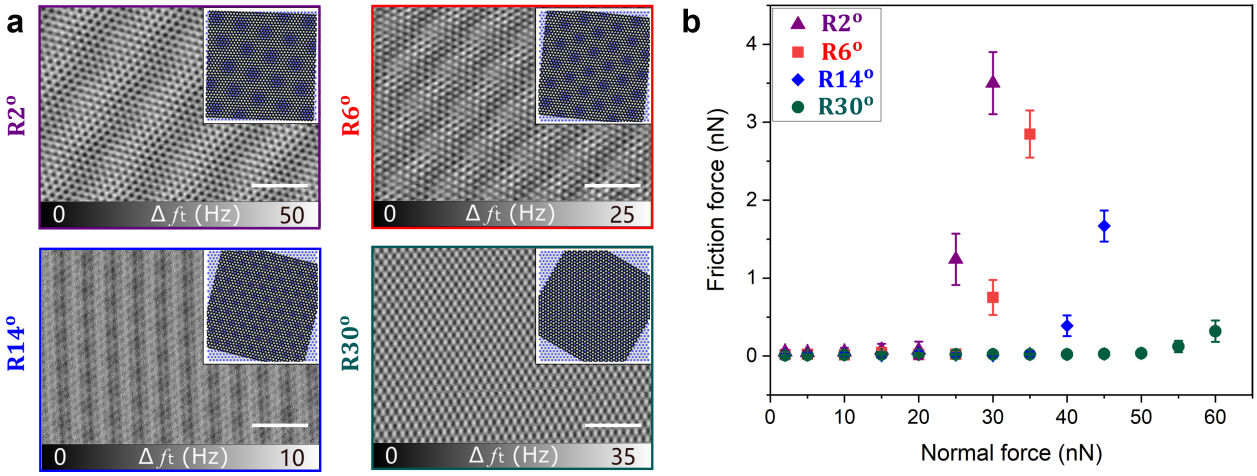

Figure 1: Topography and frictional response of graphene on Pt(111) with increasing normal loads: (**a**) nc-AFM images of different moiré patterns as defined by the torsional frequency shift Δf_t. The four twist configurations are shown in the upper right corners (graphene in black and platinum in blue, respectively). Scale bars: 2 nm. (**b**) Average friction force as a function of the normal force in the four configurations.

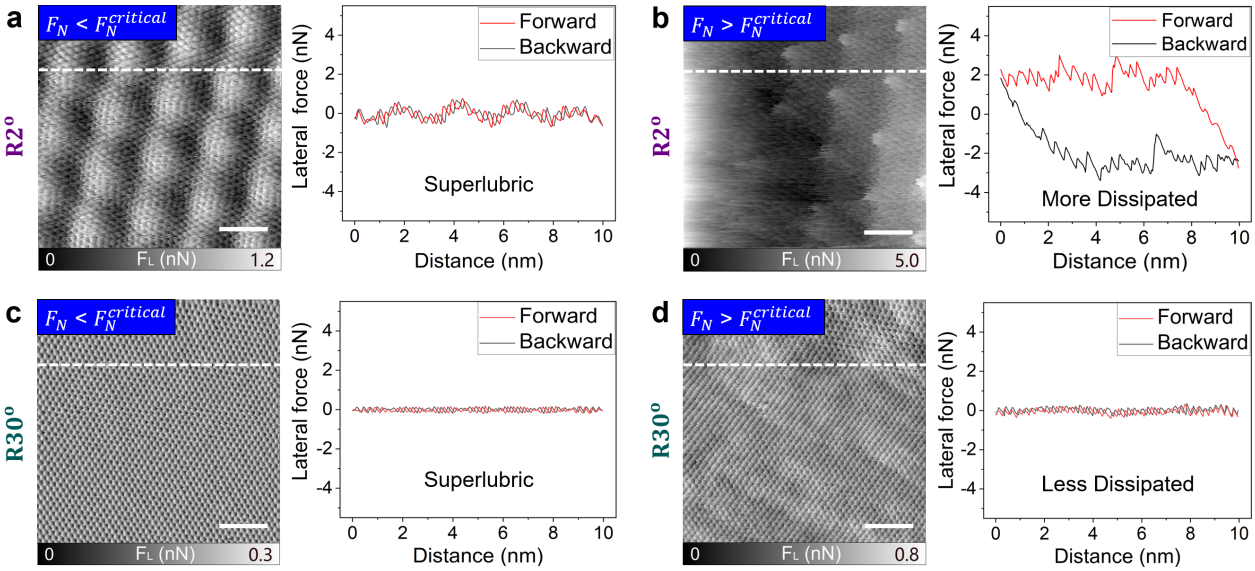

Figure 2: Lateral force images (forward scan only), and cross-sections (forward and backward) below and above the critical normal force values for: (**a**, **b**) Moiré R2^o and (**c**, **d**) Moiré R30^o. Scale bars: 2 nm.

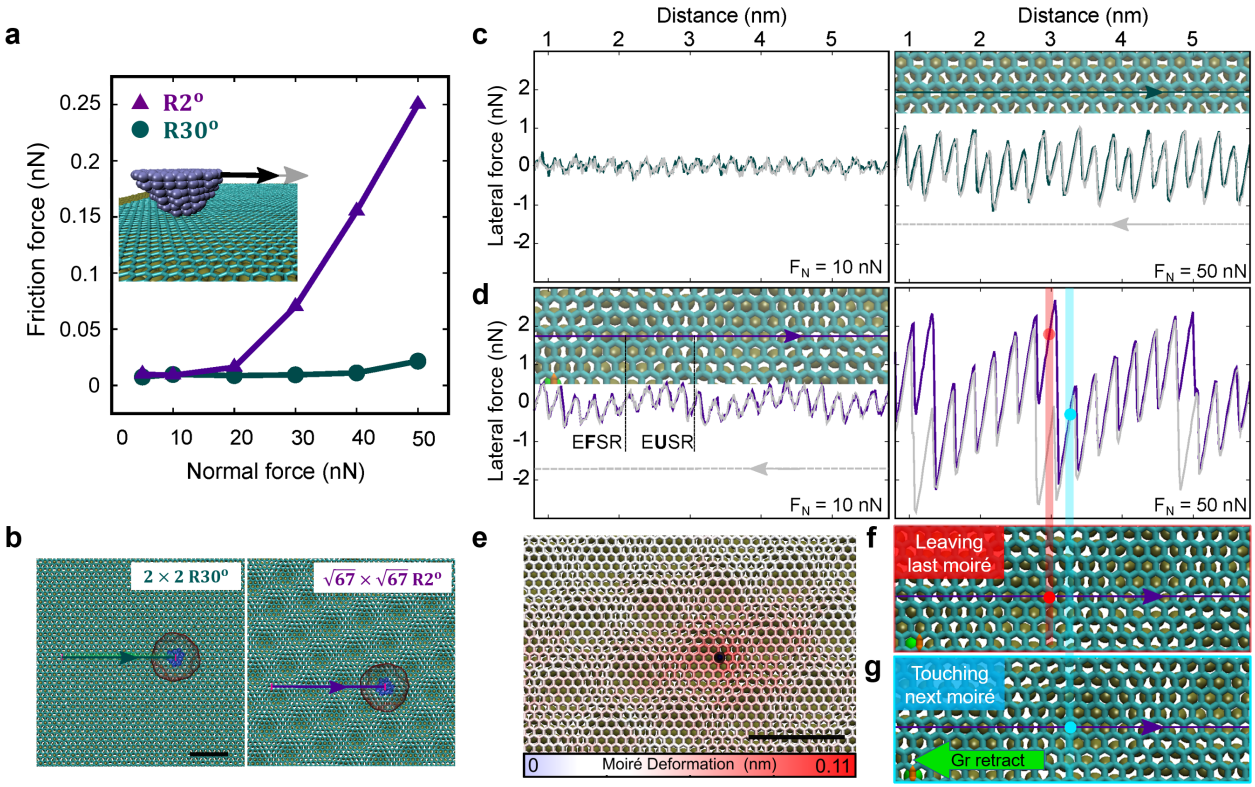

Figure 3: Dissipation mechanisms experienced by different moirés unveiled via all-atom MD. (**a**) Friction force as a function of normal load. (**b**) Top view of the considered moirés at 300 K. (**c** and **d**) Forward/backward (color/gray) lateral friction force at low (10 nN – left) and high (50 nN – right) normal loads (for R30^o (c) and R2^o (d)). The (c) and (d) insets provide the tip center-of-mass trajectory for the R30^o at all loads and R2^o at low loads, respectively. (**e**) Tip induced deformation of the R2^o at high normal loads (event highlighted in red in (d)). Maximally strained (**f**) and relaxed (**g**) R2^o moiré conformation at high loads (event highlighted in red and cyan in (d)). Scale bars: 2 nm.